

Aliphatic flexible spacer length controls photomechanical response in compact, ordered liquid crystalline polymer networks



Amir Skandani^a, J. Arul Clement^a, Stephanie Tristram-Nagle^b, M. Ravi Shankar^{a,*}

^a Swanson School of Engineering, 3700 O'Hara Street, University of Pittsburgh, Pittsburgh, PA 15261, USA

^b Biological Physics Group, Physics Department, 5000 Forbes Avenue, Carnegie Mellon University, Pittsburgh, PA 15213, USA

ARTICLE INFO

Article history:

Received 23 August 2017

Received in revised form

20 October 2017

Accepted 24 October 2017

Available online 5 November 2017

Keywords:

Photomechanical

Azobenzene

Liquid-crystal

ABSTRACT

The aliphatic spacer length connected to the rigid mesogenic cores is shown to control the structural organization and mechanical actuation in response to light-stimulus in azobenzene-functionalized liquid crystalline polymers networks. The spacer lengths in the mesogenic host (non-photochromic) and in the photo-active azobenzene-functionalized cross linker are parametrically varied to create monodomain liquid crystalline samples. A suite of thermomechanical, photomechanical and structural characterization is used to characterize the binary co-polymers. The photomechanical responses are compared by calculating a figure-of-merit – Photocompliance (Cp). This parameter, Cp, which characterizes the incremental strain generated in response to unit intensity of irradiation (W/cm^2), is found to correlate strongly with the S_{xray} order parameter and the D-spacings. We show that compact (smaller D) and higher ordering of the mesogens that result in copolymers with longer flexible spacers manifest greater photomechanical activity.

© 2017 Elsevier Ltd. All rights reserved.

1. Introduction

Liquid crystalline polymers (LCP) embedded with anisotropy at the molecular level offer programmable materials with responses tunable to an array of stimuli, including heat [1,2], light [3,4], solvent [5,6] and mechanical deformation [7]. Utilizing light to actuate LCP that are embedded with photochromic moieties such as azobenzene has attracted significant attention. This is motivated by the opportunity for enabling new system designs that use light as a contactless energy source, which can be irradiated from large stand-off distances with spatiotemporal modulation of the intensity and polarization, across length-scales. This has been utilized in photoresponsive cilia [8], customizable topographies with friction that can be tuned with light at the micrometer-scale, creation of photomechanical robots that can manipulate objects at the millimeter length-scale [9], photomobile “walkers” and motors that use multiplexed (uv and >500 nm visible light) irradiation to generate macroscopic motion [10], swimmers that can operate under photomechanically-coupled hydrodynamic conditions [11] and digital actuators that can be toggled between discrete states

using light [3].

Research efforts have examined two broad classes of azo-functionalized LCP – i) softer liquid crystal elastomers manifesting substantial actuation strains (>10%) albeit generating subdued levels of stresses [12,13] and, ii) glassy, often main-chain, azo-functionalized liquid crystalline networks (ALCN) that are capable of manifesting actuation stresses approaching the MPa-scale, but capable of modest strains (<10%) [4,14–16]. ALCN are useful for their applications as actuators in engineered applications due to their substantial photomechanical work potential and stiffness. Typically, irradiation of ALCN under ambient conditions, well below their glass transition temperature, leads to generation of significant work densities, which can be harnessed in an array of geometries [3]. A number of studies have focused on characterizing the structure-property linkages underpinning the photoactuation in ALCN. A promising class of ALCN was identified, which is characterized by host mesogens that are not photoresponsive, amongst which mesogenic photoresponsive moieties (e.g. azobenzene-based) are dispersed [17]. Photoinduced strains in such copolymers are a function of the macromolecular structure and composition in addition to the intensity and wavelength of the irradiating light. Studies on the effects of cross-linking and concentration of photoactive azobenzene molecular switches on the photo-responsiveness of the ALCN have shown that the degree of

* Corresponding author.

E-mail address: ravishm@pitt.edu (M.R. Shankar).

isomerization decreased with increasing the cross-link density, while addition of azo-based mesogen content up to 20 mol% monotonically increased the photomechanical work output [17]. The improvement in response with increasing azo content yields diminishing returns when it approaches ~35mol% due to progressive loss of nematic order at these compositions [16,18]. Increasing the cross-linking density by increasing the degree of polymerization resulted in higher stiffness, but decreased the magnitude of photostrains [19].

Following irradiation with UV light, photostrains in ALCN are generated as a result of isomerization of rod-like *trans* states, into the bent *cis* form. The associated molecular contraction is transmitted to the crosslinked polymer network, which manifests the photomechanical response in bulk. The time-scales associated with the *trans-cis* isomerization are on the order of picoseconds. However, the bulk response which is mediated by the transduction of the isomerization-induced distortion amongst the polymer network is slower by several orders of magnitude [20]. The kinetics of the isomerization and ultimately the photoresponsiveness of the actuation is underpinned by the stability of the liquid crystal system. This controls the dynamics of the photo-strain accumulation and relaxation, which is in turn a function of the structure and composition [21]. The photoresponsiveness of ALCNs is also modified by the gradient in the absorption of the light through the thickness of the sample. The absorption of the light by the photochromic moieties leads to a non-linear intensity profile, which in turn manifests a gradient in the photostrains. This results in the characteristic bending of the samples towards the light source [22].

The transduction of photonic energy into mechanical deformation in azobenzene-functionalized systems is mediated by the free-volume available for the *trans-cis* isomerization reaction [23,24], which is a function of the photochromic moiety, its conformation and its point of attachment to the polymeric chains [24]. In ALCN, the population of the *cis* and *trans*-forms of the azobenzene reaches a photostationary state in response to irradiation. The photostationary state is a statistical equilibrium, which is characterized by photomechanical strain saturation. The evolution towards this state is a function of the irradiation (intensity, wavelength and polarization), which determines the forward and reverse isomerization and reorientation of the photochromic switches. The dynamics of

such photoresponse, which generates the strain, is also associated with the generation of free volume as well as modification of the mechanical properties of the material [25]. The evolution of properties and the kinetics of the photoisomerization are intrinsically functions of the molecular flexibility in the vicinity of the photochromic moiety. This motivates us to examine whether modifying the molecular flexibility in the vicinity of the azobenzene via the choice of aliphatic spacer lengths can modulate and magnify the responsiveness of crosslinked ALCN.

Here, we first examine how the length of the aliphatic spacer connected to the azobenzene-rigid core in the crosslinker and that of the host modifies the ordering, mesogenic packing and the thermomechanical properties of the ALCN. Then, by defining a figure-of-merit – Photocompliance, we determine correlations between the photomechanical response and structural characteristics as a function of the monomer structure. We examine two host mesogens with various lengths of aliphatic spacers connected to the mesogenic core: 2-Methyl-1,4-phenylene-bis[4[3(acryloyloxy)propyloxy]benzoate] (RM257; 3-carbon aliphatic spacer) and 2-Methyl-1,4-phenylene-bis[4[6(acryloyloxy)hexyloxy]benzoate] (RM82; 6-carbon aliphatic spacer). Each of these was copolymerized with azobenzene-functionalized mesogens of various flexible spacer lengths (see Fig. 1 for structures and Fig. 1 caption for the abbreviation that refers to the various compositions). Main-chain azobenzene-based diacrylate-functionalized mesogens were synthesized and their concentration was fixed at 10 mol % for all samples. By measuring the thermal, mechanical and photoresponsiveness of the resulting polymerized films, we delineate the role of the structure of the aliphatic spacer in the azobenzene-crosslinker and the host mesogens on the photomechanical properties. In contrast to merely observing the geometric change in response to irradiation, we account for the gradients in the absorption through the thickness and calculate the saturated photostrains. To compare the responses of the various materials, we utilize photocompliance (saturation photostrain per intensity of irradiation) as the distinguishing metric. Characterizing the structural, thermomechanical and photomechanical properties via a combinatorial examination of the compositions reveals a framework for magnifying the photomechanical response.

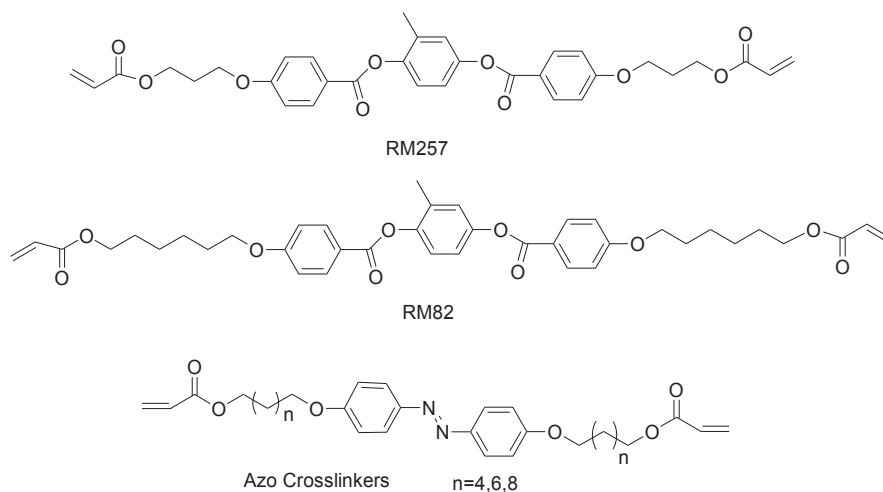


Fig. 1. Structure of host mesogens (RM257: 3C spacer and RM82: 6C spacer), which are individually copolymerized with azobenzene-functionalized cross linkers that each contain various aliphatic chain lengths. Samples denoted by RM3C, RM3C-6C, RM3-8C, RM3C-10C refer to copolymers of RM257 with azobenzene-functionalized (Azo) cross linkers containing 6C, 8C and 10C aliphatic chain lengths, respectively. RM6C, RM6C-6C, RM6-8C, RM6C-10C refer to copolymers of RM82 with azobenzene cross linkers of n= 4, 6, and 8, respectively. n+2 is the number of carbon atoms in the flexible chain of the azobenzene cross linker.

2. Materials and methods

2.1. Synthesis of 4,4-dihydroxyazobenzene (2)

A solution of p-aminophenol (10.0 g, 91.64 mmol) in diluted 1 M HCl solution (200 mL) was cooled to 0 °C by immersion in an ice bath. Next, NaNO₂ (9.34 g, 109.8 mmol) was dissolved in 150 ml of water and added drop-wise to the solution of p-aminophenol. Then, to the diazotized solution, 200 ml of pre-cooled methanol was added to. The resulting solution mixture was stirred for 1 h. Subsequently, phenol (8.62 g, 91.64 mmol) of dissolved in 65 ml of 3 M aqueous sodium hydroxide was added drop-wise and reaction mixture was stirred at room temperature for 2 h. Methanol was removed by evaporation and concentrated HCl was added to adjust pH < 5, and the resulting precipitate was collected by filtration and washed out all of the acid with water (See Scheme 1).

¹H NMR (400 MHz, DMSOd6, ppm) δ: 10.52 (s, OH) 7.70 (d, 4H, J = 8.8 Hz, ArH), 6.09 (d, 4H, J = 8.8 Hz, ArH). ¹³C NMR (100 MHz, DMSOd6, ppm) δ: 160.20, 145.72, 124.67, 116.33.

2.2. General procedure for O-alkylation

A solution of 4,4-dihydroxyazobenzene (5 g, 1 equiv), K₂CO₃ (3 equiv), and 6-chlorohexan-1-ol (2.5 equiv) were dissolved in DMF (60 mL). A trace amount of KI was added, and the reaction mixture was heated to 140 °C for 12 h. The reaction mixture was poured into water (1000 mL) and dried under vacuum so that the precipitated solid can be collected. Anhydrous MgSO₄ was used to dry the organic layer after extracting crude product with ethyl acetate. The resulting solid was fed to next step without further purification after evaporation of the solvent.

2.3. General procedure for acrylation

A solution of O-alkylation (3.0 g, 1 equiv), trimethylamine (2.5 equiv) and a trace amount of hydroquinone were dissolved in THF (60 mL) at 0 °C. The acryloyl chloride (3 equiv) was added dropwise and the reaction mixture was stirred in two stages for 1 h and 12 h at 0 °C and room temperature respectively. The reaction was quenched by adding 20 ml aqueous solution of NaHCO₃ and stirred for 30 min. The organic phase was separated and washed with water. After complete removal of the solvent purification process was performed using column chromatography (silica gel, eluent: chloroform). The remaining solid was recrystallized from ethanol yielding a yellowish powder.

2.3.1. 6-[4-(4-ethoxyphenylazo)phenoxy]hexyl acrylate

(2.45 g, 65%) ¹H NMR (400 MHz, CDCl₃, ppm) δ: 7.80 (d, 4H, J = 8.8 Hz ArH), 6.91 (d, 4H, J = 8.8 Hz ArH), 6.33 (d, 2H, J = 17.6 Hz

vinyl), 6.05 (dd, 2H, J = 10.4 Hz vinylic), 5.74 (d, 2H, J = 10.4 Hz vinylic), 4.10 (t, 4H, J = 6.6 Hz, OCH₂), 3.96 (t, 4H, J = 6.4 Hz, OCH₂), 1.78–1.74 (m, 4H), 1.67–1.61 (m, 4H), 1.48–1.37 (m, 8H). ¹³C NMR (100 MHz, CDCl₃, ppm) δ: 166.35, 161.27, 146.63, 130.59, 128.59, 124.50, 114.72, 68.12, 64.52, 29.11, 28.57, 25.76.

2.3.2. 8-[4-(4-ethoxyphenylazo)phenoxy]octyl acrylate

(2.51 g, 68%) ¹H NMR (400 MHz, CDCl₃, ppm) δ: 7.79 (d, 4H, J = 9.2 Hz ArH), 6.91 (d, 4H, J = 9.2 Hz ArH), 6.32 (dd, 2H, J = 17.2 Hz vinylic), 6.05 (dd, 2H, J = 10.4 Hz vinylic), 5.74 (dd, 2H, J = 12.0 Hz vinylic), 4.08 (t, 4H, J = 6.6 Hz, OCH₂), 3.96 (t, 4H, J = 6.6 Hz, OCH₂), 1.78–1.71 (m, 4H), 1.62–1.59 (m, 4H), 1.43–1.41 (m, 4H), 1.39–1.31 (m, 12H). ¹³C NMR (100 MHz, CDCl₃, ppm) δ: 166.36, 161.14, 146.96, 130.48, 128.64, 124.30, 114.66, 68.24, 64.65, 29.25, 29.17, 28.60, 25.96, 25.87.

2.3.3. 10-[4-(4-ethoxyphenylazo)phenoxy]decyl acrylate

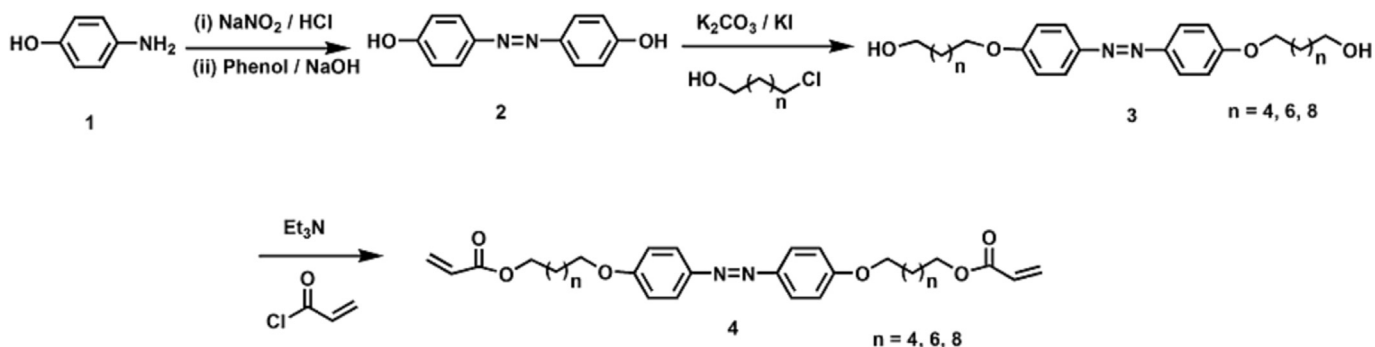
(2.60 g, 72%) ¹H NMR (400 MHz, CDCl₃, ppm) δ: 7.79 (d, 4H, J = 8.8 Hz ArH), 6.91 (d, 4H, J = 9.2 Hz ArH), 6.32 (dd, 2H, J = 17.6 Hz vinylic), 6.05 (dd, 2H, J = 10.6 Hz vinylic), 5.74 (dd, 2H, J = 10.4 Hz vinylic), 4.08 (t, 4H, J = 6.6 Hz, OCH₂), 3.96 (t, 4H, J = 6.4 Hz, OCH₂), 1.77–1.70 (m, 4H), 1.63–1.58 (m, 4H), 1.41–1.38 (m, 4H), 1.36–1.25 (m, 20H). ¹³C NMR (100 MHz, CDCl₃, ppm) δ: 166.36, 161.16, 146.94, 130.44, 128.66, 124.30, 114.66, 68.30, 64.71, 29.46, 29.43, 29.35, 29.23, 28.61, 26.02, 25.92.

2.4. Polarized optical microscopy and differential scanning calorimetry of monomers

Table 1 summarizes different monomer mixture compositions that were tested using a Perkin Elmer Diamond differential scanning calorimeter (DSC) and hot stage polarized optical microscopy (POM) to obtain the characteristic temperature of each mixture (i.e. melting temperature and nematic to isotropic phase transformation). Differential scanning calorimetry tests were performed with a heating mode with 5 °C/min and under nitrogen environment.

2.5. Monodomain liquid crystal polymer samples

All six compositions outlined in Table 1 were added with Irgacure 784, (photoinitiator, 1 wt % of the total reactants) and heated at (130 °C) in the isotropic phase. The molten mixture was then infiltrated into the parallel rubbed polyimide-coated glass cells of 50 μm gap via capillarity. The parallel anchoring conditions on either side of the cell ensure the creation of monodomain alignment parallel to the rubbing direction. The filled cells were slowly cooled down at – 1° C/min to the nematic phase while T_p/T_{NI} ratio was fixed at 0.95, to attempt to maintain a comparable order



Scheme 1. Synthesis of azobenzene-functionalized cross-linkers with spacers of various aliphatic spacer lengths.

Table 1
The monomer composition and T_{NI} temperature of different samples.

Sample	Composition	T_{NI} (°C)
RM3C-6C	RM257(90 Mol%) + Azobenzene crosslinker (n+2 = 6) (10 Mol%)	115
RM3C-8C	RM257(90 Mol%) + Azobenzene crosslinker (n+2 = 8) (10 Mol%)	113
RM3C-10C	RM257(90 Mol%) + Azobenzene crosslinker (n+2 = 10) (10 Mol%)	107
RM6C-6C	RM82(90 Mol%) + Azobenzene crosslinker (n+2 = 6) (10 Mol%)	109
RM6C-8C	RM82(90 Mol%) + Azobenzene crosslinker (n+2 = 8) (10 Mol%)	108
RM6C-10C	RM82(90 Mol%) + Azobenzene crosslinker (n+2 = 10) (10 Mol%)	109

parameter across all samples [26,27]. T_p is the polymerization temperature and T_{NI} is the nematic-isotropic transition temperature of the monomer mixture. Edmund MI-150 high-intensity illuminator was utilized to irradiate the samples with a cutoff filter ($1 \geq 420$ nm) in order to photopolymerize the samples for 1 h. Cells were opened using scalpel to reveal the free-standing, mono-domain ALCN films.

2.6. Wide-angle X-ray scattering (WAXS)

WAXS data were collected using the Rigaku rotating anode RUH3R. Samples were prepared by cutting a narrow strip (2×10 mm) from the thin polymer sheets, in the direction parallel to the rubbing direction (nematic director). These strips were fixed onto the axle of a precision motor (AirProducts, Inc.,) with double-stick tape, so that 3 mm extended out from the axle. This extension was X-rayed at 90° to the nematic director while the 2 mm wide sample was rapidly rotated in the X-ray beam from -5 to 5° . Cu K α radiation with $\lambda = 1.5418$ Å was used; beam size was 0.5×0.5 mm, focused with a Xenocs Fox2D focusing collimator. 2D images were collected on a Rigaku Mercury CCD detector in 5 min dezingered scans. The sample-to-CCD distance was ~ 100 mm, in three separate runs, calibrated with Teflon powder ($D = 4.898$ Å).

In order to carry out the WAXS data analysis, the images were first rotated counterclockwise by 90° and flipped horizontally. The WAXS scattering was then primarily on the equator in the right-hand quadrant. This orientation is required for data analysis with a MATLAB liquid-crystal fitting program [28]. This program determines S_{xray} , a chain order parameter, similar to an NMR order parameter [29]. More details about the WAXS data collection and analysis are given in Supplementary Materials.

2.7. Thermomechanical characterization

A Perkin Elmer 8000 dynamic mechanical analysis (DMA) was utilized to measure the mechanical properties of the monodomain samples along the nematic director, including storage and loss moduli and $\tan \delta$. The DMA experiments were carried out in strain control mode using a tension fixture with frequency of 1 Hz and temperature sweep from room temperature to 150°C . DMA samples were prepared in the form of 25 mm \times 1 mm rectangles (longer axes parallel to the nematic director) and mounted with 0.1 N of pre-stretching force to eliminate possible slack. Results were recorded and analyzed as a function of the composition of the films.

2.8. Photomechanical characterization

The absorption coefficient of each sample was measured using CRAIC QDI 2010 UV-VIS-NIR instrument in 200 – 800 nm range. Rectangular samples with 25 mm length and 1 mm width were excised from the original films with the longer axes parallel to the nematic director. Samples were then clamped from one end and irradiated uniformly with 30 mW/cm [2] of un-polarized 375 nm

UV source until the photomechanical strain saturates and progressive bending with continued irradiation stopped. A prior flat sample characteristically bends towards the light and develops a curvature due to the photostrains. Under these irradiation intensities, negligible photothermal effects are expected and the actuation essentially occurs photochemically under nominally ambient conditions [30]. The resultant deformations in the samples were recorded with a USB camera positioned at a right angle and in plane with the sample to observe the development of the photo-strained geometry. The recorded images were then sliced to 1 frame per 2 s and were analyzed using a home-built MatLab code to extract the evolution of the curvature of the sample throughout the experiment. The saturation value of the curvature is used to characterize the photomechanical response.

3. Results and discussion

Fig. 2 shows the DSC peaks of different monomer mixtures along with their hot stage polarized optical microscopy images between each peak. It can be seen that by increasing the aliphatic chain length the nematic to isotropic transformation temperature (T_{NI}) decreases while the presence of azobenzene crosslinker reduces the melting temperature irrespective of its structure. The effect of the spacer length on the T_{NI} and the melting temperature is consistent with prior studies [31,32]. The absorption coefficients (Napierian) of the polymer film compositions from Table 1 are shown in Fig. 3 as a function of wavelength ranging from 200 nm to 800 nm. We note a marginal decline in the absorption coefficients of samples with increasing carbon chain length except, RM3C-10C. Table 2 lists the coefficient at 375 nm at which we examine the photomechanical responses.

Representative thermo-mechanical responses of the various composition films is shown in Fig. 4. The reported storage modulus (E') from DMA tests (Fig. 4a) is a measure of the sample's stiffness along the nematic director. It can be seen that E' at room temperature is primarily determined by the host mesogen, where higher stiffness is observed for the shorter spacer length (RM257) (Table 2). Both storage modulus and loss modulus (E'') (Fig. 4b) drop sharply during glass transition before reaching a plateau at higher temperatures. Similar behavior of azo-LCNs have been reported elsewhere [19]. From $\tan \delta$ plot of the samples (Fig. 4c), a relatively broad glass transition can be observed for all of the samples, which is typical [14,15]. The cross-link density was calculated using equation (1) where T_{high} and E'_{high} are at temperature 50°C higher than T_g and its corresponding storage modulus respectively [19]:

$$V_e = E'_{high} / 3RT_{high} \quad (1)$$

The thermomechanical properties are shown in Table 2 for the various compositions.

The wide-angle X-ray scattering data are shown in Fig. 5. These are 2D CCD images of slightly more than one quadrant of the entire image, where white pixels indicate higher X-ray scattering intensity. The X-ray beam is covered by a semi-transparent

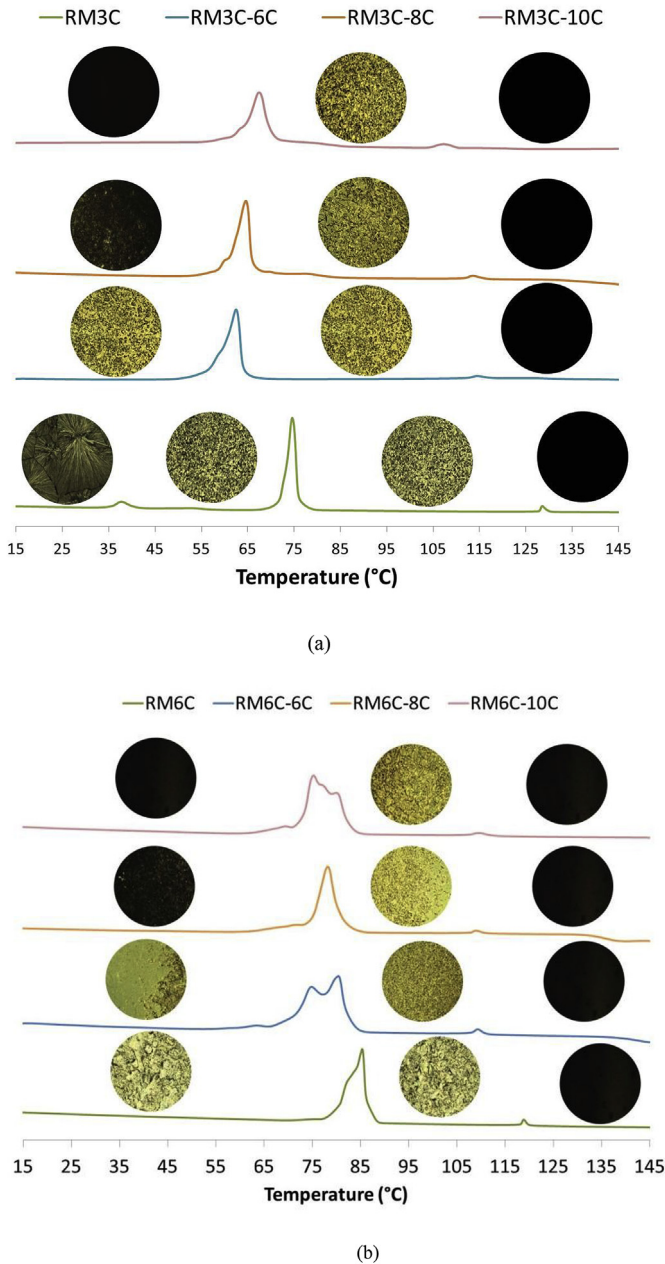


Fig. 2. DSC curves of different compositions in the form of powder mixture before polymerization along with their POM images a) RM257 and b) RM82. Insets illustrates the POM images (crossed polarizers) measured at the corresponding temperatures.

molybdenum strip in the lower left corner. Absence of lamellar scattering close to the beam confirms that there is no smectic ordering in these samples. Most of the scattered intensity is located on the meridian; the width and decrease of this intensity in an azimuthal direction are used to quantitate S_{xray} , an order parameter similar to an NMR order parameter (Ref. 33, 34). As shown in Fig. 5, a bright, compact reflection near 1.5 \AA^{-1} in q_z is indicative of a well-ordered polymer chain; this occurred in all samples. S_{xray} order parameters and D-spacings are summarized in Table 2. The consequences of these order parameters and D-spacing values will be discussed below. In addition to the major, bright meridional reflection resulting from interactions of the main polymer chain backbone, there is a very weak reflection at $\sim 0.8 \text{ \AA}^{-1}$, with a D-spacing of $\sim 8.4 \text{ \AA}$ in all of the samples. The origin of this small

reflection is unknown.

The photomechanical response of the samples under UV irradiation is shown in Fig. 6. Instead of merely comparing the final curvatures of the sample, we seek to abstract a photomechanical figure-of-merit – the photocompliance (C_p). C_p is defined as the contractile strain accumulated by an element of the material along the nematic director when exposed to irradiation of unit intensity (W/cm [2]). Normalizing the strain generated with respect to the intensity allows the results to hold broader applicability, while allowing a one-to-one comparison between the various materials. When a nominally flat film is irradiated, the absorption through the thickness generates an intensity gradient through the film (Fig. 7). Strains generated within the monodomain film at any given distance x from the surface scale with the intensity $I(x)$:

$$I(x) = I_0 e^{-\mu x} \quad (2)$$

μ is the absorption coefficient as a function of the composition and I_0 is the incident irradiation of the light at the surface of the sample. Note that the mole% of azobenzene is fixed across all compositions in this study.

The photostrain value at depth x is determined by C_p value of the composition, where:

$$\varepsilon_{ph} = C_p I(x) \quad (3)$$

The mechanical deformation manifesting bending that leads to curvature of radius r can be described by a strain field ε_b , which can be written as [15]:

$$\varepsilon_b = \frac{x}{r} + c \quad (4)$$

where, h is the thickness of the sample and $x \in [0, h]$ and c is the stretching strain. Imaging of the sample is used to measure r in our experiments by characterizing the deformed geometry.

The stress σ_y , which manifests the bending is given by Ref. [15]:

$$\sigma_y = E' \left(\frac{x}{r} + c - \varepsilon_{ph} \right), \quad (5)$$

where E' is the storage modulus (from DMA) along the nematic director.

Enforcing equilibrium for force ($\int_0^h \sigma_y dx = 0$) and moments ($\int_0^h x \sigma_y dx = 0$), the following expression was derived using Mathematica. The measured radius of curvature (r) and the curvature (κ) are:

$$r = 1/\kappa = \frac{h^3 \mu^2 e^{\mu h}}{6I_0 C_p (\mu h + \mu h e^{\mu h} + 2 - 2e^{\mu h})} \quad (6)$$

Hence, the C_p value as a function of compositions can be back calculated from an imaging-based measurement of the final curvature κ of the irradiated sample using:

$$C_p = \frac{\kappa h^3 \mu^2 e^{\mu h}}{6I_0 (\mu h + \mu h e^{\mu h} + 2 - 2e^{\mu h})} \quad (7)$$

Equation (7) and the saturated curvatures in Fig. 6 for the various compositions were used to calculate the absolute value of C_p (Table 2). Some overarching trends are observed from these results. Longer flexible spacer lengths in both the host and the azobenzene cross linkers result in larger values of C_p . Thus, for unit photon flux, RM6C-10C produces the greatest strains ($C_p = 0.3$), while RM 3C-6C produces the smallest ($C_p = 0.13$). The difference

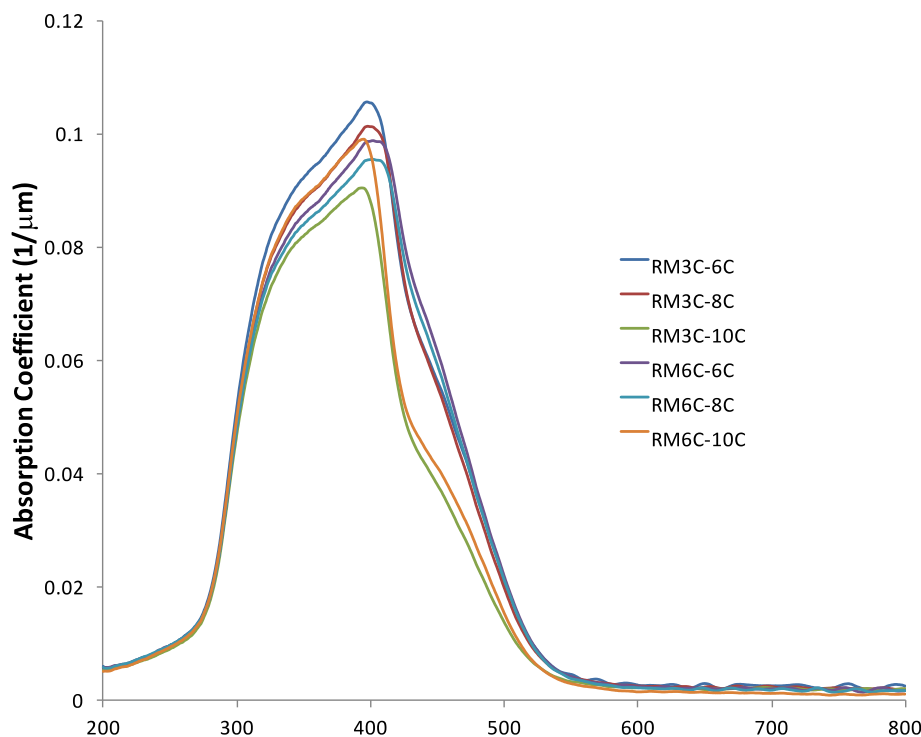


Fig. 3. Absorption coefficient of polymerized samples measured between 200 and 800 nm at room temperature.

Table 2

Photo- and thermo-mechanical properties of the samples.

	E (GPa) @25 °C	Cross-link density ($\frac{\text{mol}}{\text{dm}^3}$)	Glass Transition T_g (°C)	Absorption Coefficient (μ) at 375 nm (cm^{-1})	Sxray	D-spacing (Å)	C_p ($\frac{\text{nm}^2}{\text{W}}$)
RM3C-6C	2.63	20	109	991	0.38 ± 0.01	4.49 ± 0.01	0.13
RM3C-8C	2.32	19.8	92	949	0.35 ± 0.01	4.49 ± 0.02	0.14
RM3C-10C	2.22	15.35	87	874	0.453 ± 0.004	4.52 ± 0.01	0.18
RM6C-6C	2.08	30	77	922	0.42 ± 0.01	4.47 ± 0.01	0.21
RM6C-8C	1.90	28	72	898	0.51 ± 0.02	4.46 ± 0.01	0.26
RM6C-10C	1.75	22.33	72	949	0.57 ± 0.01	4.45 ± 0.01	0.30

between the two compositions is by a factor greater than two. Indeed, the glass transition also shows a decline with increasing spacer length, which is consistent with prior reports [33]. Another factor that contributes to the magnified response in the RM82 (6C) systems is the deeper penetration of light in this system, in comparison to the RM257 (3C) [34]. This can magnify the isomerization of the azobenzene and result in greater photoresponsiveness.

The WAXS data indicate while all systems are predominantly ordered, differences in the order parameter are observed, even though the ratio of the polymerization temperature with respect to the nematic-isotropic transition of the monomer mixture was fixed at 0.95 for all compositions. The S_{xray} values for the RM3C samples averaged to 0.40, which shows that they are not as well-ordered as the RM6C samples (average $S_{\text{xray}} = 0.50$). These order parameters are similar to the highest order parameter of 0.47 determined for LCN-16.6, which is 98.4% RM82 (equivalent to RM6C series in this work) in the literature [35]. In addition, all of the RM6C samples had smaller D-spacings (average = 4.46 Å) than the RM3C samples (average = 4.50 Å), indicating a tighter packing. In an effort to understand how chain ordering and D-spacing are correlated with photoresponse (C_p), two additional comparisons were made. When C_p is plotted vs. S_{xray} order parameter as shown in Fig. 8 (a), a

dependence of C_p on S_{xray} is shown; i.e., the photoresponse increases in more ordered samples. When comparing D-spacing and C_p as shown in Fig. 8 (b), the photoresponse is larger when the sample has a smaller D-spacing. These results suggest that the maximal photoresponse occurs when the polymer sample is well-ordered and also compact. In the case of RM6C-10C, the strain in an infinitesimal element of the material at the surface, which is directly exposed to the incident irradiation, can be calculated as $\sim C_p I_0 = 0.9\%$. This is a significant value of strain in a glass ALCN with a storage modulus of ~ 1.75 GPa that is irradiated with a modest intensity of light. It has been suggested that photoresponsiveness is mainly controlled by the free volume distribution around the photochromic moiety, which is different from its usual random distribution. During photoisomerization, there can be a redistribution of free volume [24]. It is perhaps that the isomerization proceeds most efficiently with a well-ordered, compact starting configuration. Starting from this configuration, *trans-cis* photoisomerization generates disordering and concomitant photomechanical strains most efficiently.

Instructive ideas can be drawn from analogous strain generation via thermally-driven order-disorder transitions in liquid crystalline polymers. In glassy LCP that are thermally-responsive, modest

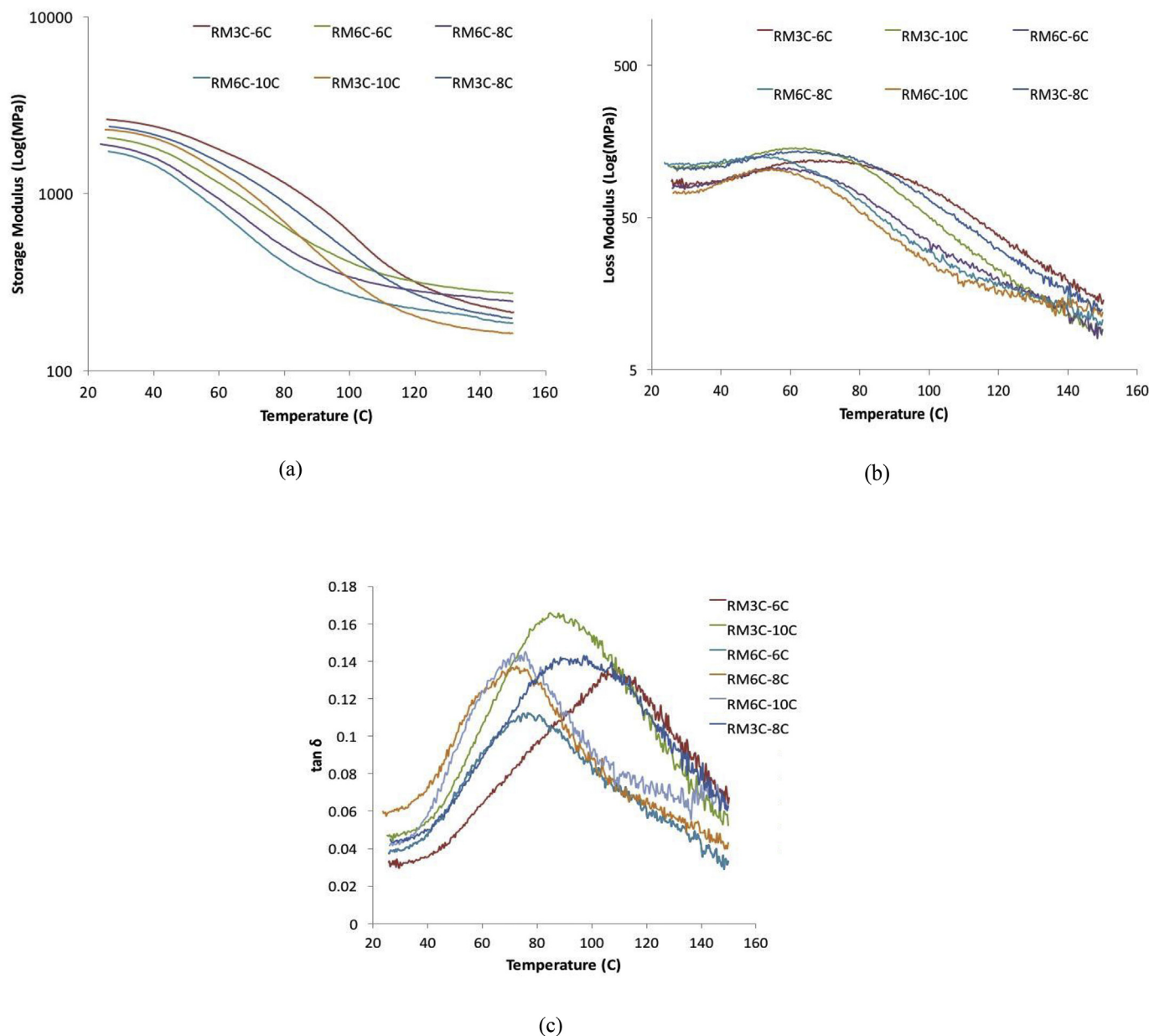


Fig. 4. Thermomechanical properties of ALCN as a function of monomer structure. DMA experiments were conducted parallel to the nematic director with 1HZ frequency, a) Elastic modulus (E'), b) Loss modulus (E''), c) $\tan(\delta)$.

changes (5%) in the order parameter account for the strain generation. In such systems, no transition to the isotropic state occurs, although the responsiveness is affected by the length of the aliphatic spacer that is attached to the mesogenic core; the longer aliphatic spacers correlate with greater responsiveness [27]. It has been shown that longer aliphatic spacer length correlates with lower glass transition temperature (T_g) [33]. Indeed, photomechanical strain generation in glassy ALCN well below T_g does not require the same level of segmental mobility that underpins thermomechanical strain generation. But, higher segmental mobility that emerges with longer flexible spacers can be expected to magnify photomechanical response. On the other hand, it is known that the length of the flexible spacer affects the stability of the nematic state [36], which determines the process window available for polymerizing the mesogens to inherit the molecular ordering. Utilizing longer flexible spacers in the azobenzene-functionalized

cross-linkers can adversely modify the achievement of nematic ordering in mixtures created with the host mesogens (e.g. RM257/RM82). This constrains the ability to indefinitely magnify the photoresponse by using longer flexible spacers.

Segmental mobility of the polymer network has an effect on the isomerization efficiency. It has also been shown that changing the aliphatic chain length in the spacer can affect the efficiency of the *trans-cis* isomerization as a function of the polymer network in temperatures below their T_g [37–39]. Flexibility of the molecular chains enabled by spacers attached to the mesogenic cores offers the necessary rotational flexibility required for reorientation [40]. This is clearly illustrated in Fig. 9, where the T_g of the various samples is plotted against C_p . It is clear that greater the aliphatic chain length, lower is the T_g and greater is the photoresponse. It is noteworthy that this photoresponse also goes hand-in-hand with smaller D-spacing and higher S_{xray} when

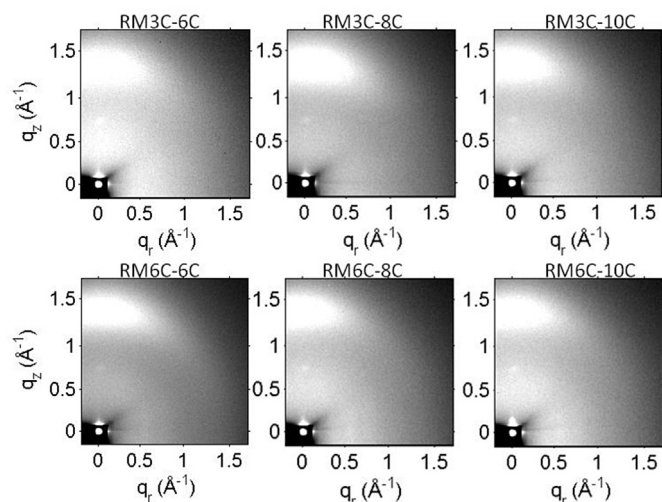


Fig. 5. 2D CCD WAXS images at grazing angle-of-incidence to ALCN oriented 90° to the alignment direction.

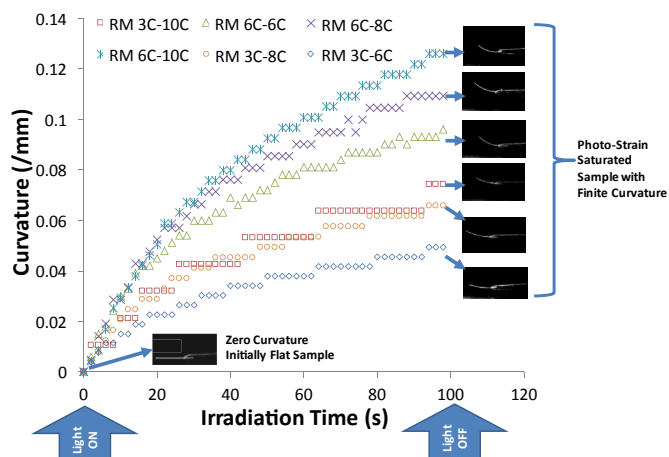


Fig. 6. Photomechanical bending experiments of samples under 30 mW/cm^2 [2] of unpolarized 375 nm UV irradiation.

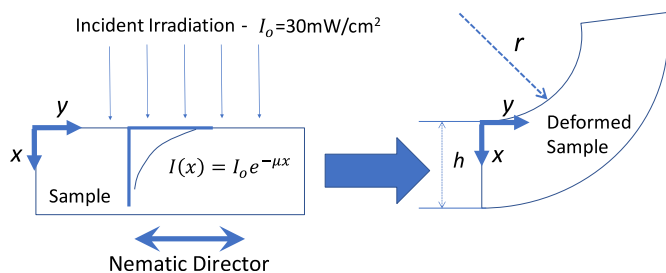
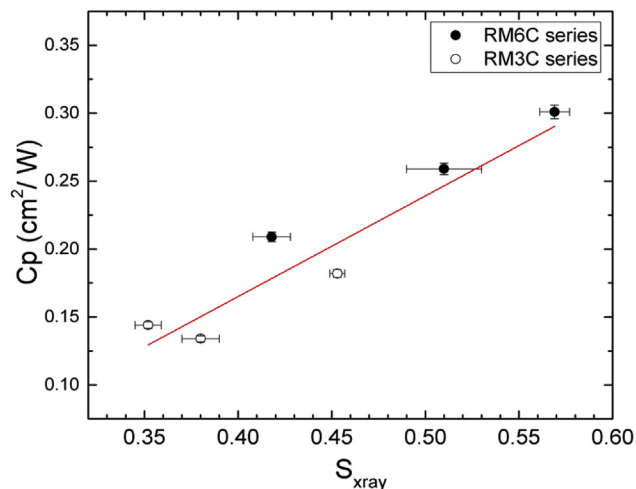


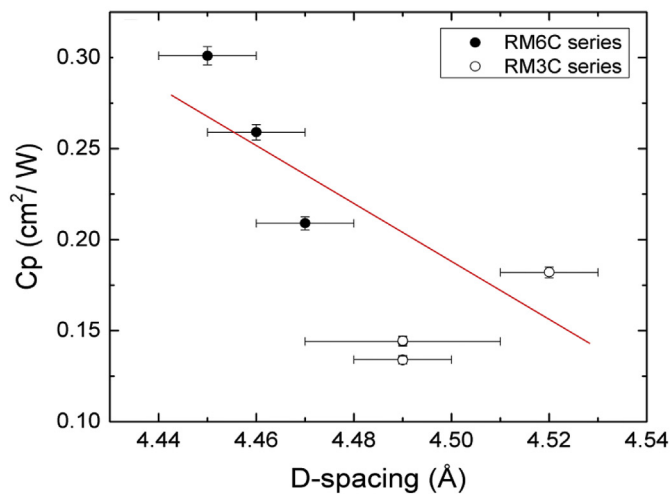
Fig. 7. Schematic of the geometric evolution, which was used to derive a figure-of-merit, photocompliance C_p , which is the normalized strain accumulated per unit intensity (W/cm^2 [2]) of incident irradiation.

the aliphatic spacer length is made longer.

An important caveat emerges from the observation that the reorientation during isomerization of azobenzene involves predominantly localized molecular distortions involving molecular segments in the vicinity of the photochromic switch, which limits role for the structure to the spacer itself [41]. While the kinetics of



(a)



(b)

Fig. 8. (a) Photoresponse (C_p) vs. S_{xray} . S_{xray} errors were obtained by measuring two separate pieces of the same polymer film. (b) Photoresponse (C_p) vs. WAXS D-spacing. D-spacing errors were obtained by measuring two separate pieces of the same polymer film.

the *trans* to *cis* isomerization plays a deterministic role in the responsiveness, so does the kinetics of the back-reaction. The *cis-trans* back isomerization rate is lower for azobenzene embedded in polymeric hosts with longer spacers [37]. This effect can enable the generation of a greater concentration of the *cis* form in a photo-stationary state, which results in greater photomechanical strains. While remaining cognizant of the complex role of the molecular structure on the photoresponse, we also note the observed correlations between the photomechanical output and the material's bulk mechanical properties. The monomer structure (host and the azobenzene cross linkers) controls the resulting storage/loss moduli and cross-link densities. The photoresponse that is observed is known to be highly correlated with the mechanical properties of the matrix [42]. If the interplay of the molecular structure with the modulus and photoinduced strain can be delineated, a framework can emerge for modulating the property combinations. In particular, if the photostrain generation can be enhanced, while retaining a high modulus, material systems can emerge that offer work densities that allow their utilization in

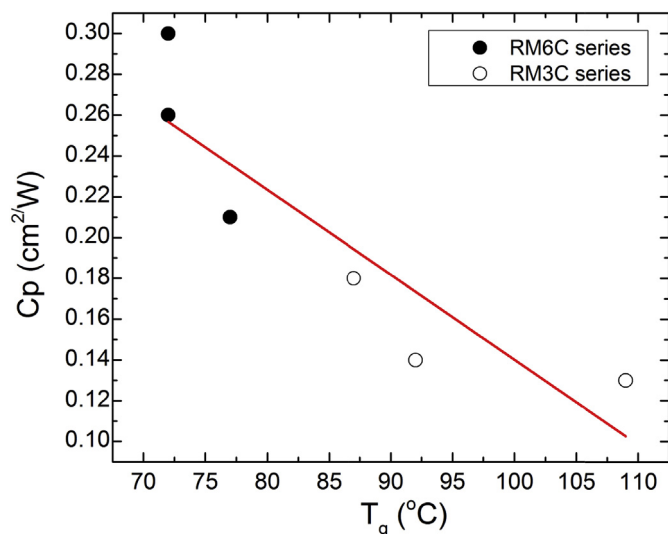


Fig. 9. Decline in T_g with increasing spacer lengths correlates with greater C_p .

practical light-responsive actuators. Such material property enhancements can allow light-sensitive actuation to complement thermally-responsive counterparts fabricated from liquid crystalline systems. For example, modifying the flexible spacer has been shown to double the photocompliance, even when the mole % of azobenzene is held constant. Thus, engineering the local molecular environment magnifies the resulting photomechanical actuation.

4. Conclusions

An exploration of the photomechanical response as a function of the aliphatic spacer length attached to the mesogenic core in azobenzene-functionalized liquid crystalline polymer networks was undertaken. The spacer length connected to the azobenzene core as well as that of the non-photochromic host mesogens were varied. The azobenzene concentration was held constant among the binary combinatorial co-polymers and ratio of the temperature of polymerization to that of the nematic-isotropic transition of the monomer mixtures was fixed. Isolating the effect of the monomer structure on the structural characteristics resulted in identifying a route of magnifying the photostrain generation by incorporating greater flexibility in the networks using longer aliphatic spacers. Additionally, a figure of merit – photocompliance was calculated from experiments that encapsulated the photostrain magnitude along the nematic director per unit irradiation intensity. The photocompliance was found to strongly correlate with the higher order parameters, lower T_g and smaller D-spacing – compact, flexible, well-ordered nematic networks produce the greatest photostrains. This offers a motif for rationally designing GPa-stiffness glassy, macromolecular networks with ordered molecular switches, where the photomechanical strain generation can be magnified, even under ambient conditions and modest irradiation intensities.

Acknowledgement

MRS acknowledges support from the Air Force Office of Scientific Research (FA9550-14-1-0229) and the National Science Foundation (#1435489). STN acknowledges the Physics department at Carnegie Mellon University for support for this work.

Appendix A. Supplementary data

Supplementary data related to this article can be found at <https://doi.org/10.1016/j.polymer.2017.10.050>.

References

- [1] T.J. White, M.E. McConney, T.J. Bunning, Dynamic color in stimuli-responsive cholesteric liquid crystals, *J. Mater. Chem.* 20 (44) (2010) 9832–9847.
- [2] J. Küpfer, H. Finkelmann, Liquid crystal elastomers: influence of the orientational distribution of the crosslinks on the phase behaviour and reorientation processes, *Macromol. Chem. Phys.* 195 (4) (1994) 1353–1367.
- [3] M.R. Shankar, M.L. Smith, V.P. Tondiglia, K.M. Lee, M.E. McConney, D.H. Wang, L.-S. Tan, T.J. White, Contactless, photoinitiated snap-through in azobenzene-functionalized polymers, *Proc. Natl. Acad. Sci.* 110 (47) (2013) 18792–18797.
- [4] Y. Yu, M. Nakano, T. Ikeda, Photomechanics: directed bending of a polymer film by light, *Nature* 425 (6954) (2003), 145–145.
- [5] L.T. de Haan, J.M. Verjans, D.J. Broer, C.W. Bastiaansen, A.P. Schenning, Humidity-responsive liquid crystalline polymer actuators with an asymmetry in the molecular trigger that bend, fold, and curl, *J. Am. Chem. Soc.* 136 (30) (2014) 10585–10588.
- [6] T. Kamal, S.-Y. Park, A liquid crystal polymer based single layer chemo-responsive actuator, *Chem. Commun.* 50 (16) (2014) 2030–2033.
- [7] H. Aoyama, Y. Yamazaki, N. Matsuura, H. Mada, S. Kobayashi, Alignment of liquid crystals on the stretched polymer films, *Mol. Cryst. Liq. Cryst.* 72 (4) (1981) 127–132.
- [8] H. Yang, G. Ye, X. Wang, P. Keller, Micron-sized liquid crystalline elastomer actuators, *Soft Matter* 7 (3) (2011) 815–823.
- [9] F. Cheng, R. Yin, Y. Zhang, C.-C. Yen, Y. Yu, Fully plastic microrobots which manipulate objects using only visible light, *Soft Matter* 6 (15) (2010) 3447–3449.
- [10] M. Yamada, M. Kondo, R. Miyasato, Y. Naka, J.-i. Mamiya, M. Kinoshita, A. Shishido, Y. Yu, C.J. Barrett, T. Ikeda, Photomobile polymer materials—various three-dimensional movements, *J. Mat. Chem.* 19 (1) (2008) 60–62.
- [11] M. Camacho-Lopez, H. Finkelmann, P. Palffy-Muhoray, M. Shelley, Fast liquid-crystal elastomer swims into the dark, *Nat. Mater.* 3 (5) (2004) 307–310.
- [12] H. Finkelmann, E. Nishikawa, G. Pereira, M. Warner, A new opto-mechanical effect in solids, *Phys. Rev. Lett.* 87 (1) (2001) 015501.
- [13] J. Cviklinski, A. Tajbakhsh, E.M. Terentjev, UV isomerisation in nematic elastomers as a route to photo-mechanical transducer, *Eur. Phys. J. E* 9 (1) (2002) 427–434.
- [14] K.D. Harris, R. Cuyppers, P. Scheibe, C.L. van Oosten, C.W. Bastiaansen, J. Lub, D.J. Broer, Large amplitude light-induced motion in high elastic modulus polymer actuators, *J. Mater. Chem.* 15 (47) (2005) 5043–5048.
- [15] C. Van Oosten, K. Harris, C. Bastiaansen, D. Broer, Glassy photomechanical liquid-crystal network actuators for microscale devices, *Eur. Phys. J. E* 23 (3) (2007) 329–336.
- [16] Y. Yu, M. Nakano, A. Shishido, T. Shiono, T. Ikeda, Effect of cross-linking density on photoinduced bending behavior of oriented liquid-crystalline network films containing azobenzene, *Chem. Mater.* 16 (9) (2004) 1637–1643.
- [17] M. Kondo, M. Sugimoto, M. Yamada, Y. Naka, J.-i. Mamiya, M. Kinoshita, A. Shishido, Y. Yu, T. Ikeda, Effect of concentration of photoactive chromophores on photomechanical properties of crosslinked azobenzene liquid-crystalline polymers, *J. Mater. Chem.* 20 (1) (2010) 117–122.
- [18] Y. Wu, Q. Zhang, A. Kanazawa, T. Shiono, T. Ikeda, Y. Nagase, Photoinduced alignment of polymer liquid crystals containing azobenzene moieties in the side chain. 5. Effect of the azo contents on alignment behavior and enhanced response, *Macromolecules* 32 (12) (1999) 3951–3956.
- [19] K.M. Lee, H. Koerner, R.A. Vaia, T.J. Bunning, T.J. White, Relationship between the photomechanical response and the thermomechanical properties of azobenzene liquid crystalline polymer networks, *Macromolecules* 43 (19) (2010) 8185–8190.
- [20] Y. Zhao, T. Ikeda, *Smart Light-responsive Materials: Azobenzene-containing Polymers and Liquid Crystals*, John Wiley & Sons, 2009.
- [21] T. Fischer, L. Läscher, J. Stumpe, S. Kostromin, Photoinduced optical anisotropy in films of photochromic liquid crystalline polymers, *J. Photochem. Photobiol. A Chem.* 80 (1) (1994) 453–459.
- [22] D. Corbett, M. Warner, Bleaching and stimulated recovery of dyes and of photocalifiers, *Phys. Rev. E* 77 (5) (2008) 051710.
- [23] C.D. Eisenbach, Effect of polymer matrix on the cis-trans isomerization of azobenzene residues in bulk polymers, *Die Makromol. Chem.* 179 (10) (1978) 2489–2506.
- [24] G.S. Kumar, D. Neckers, Photochemistry of azobenzene-containing polymers, *Chem. Rev.* 89 (8) (1989) 1915–1925.
- [25] H.K. Kim, X.S. Wang, Y. Fujita, A. Sudo, H. Nishida, M. Fujii, T. Endo, Reversible photo-mechanical switching behavior of azobenzene-containing semi-interpenetrating network under UV and visible light irradiation, *Macromol. Chem. Phys.* 206 (20) (2005) 2106–2111.
- [26] D.J. Broer, G.N. Mol, Anisotropic thermal expansion of densely cross-linked oriented polymer networks, *Polym. Eng. Sci.* 31 (9) (1991) 625–631.
- [27] G.N. Mol, K.D. Harris, C.W. Bastiaansen, D.J. Broer, Thermo-mechanical responses of liquid-crystal networks with a splayed molecular organization,

- Adv. Funct. Mater. 15 (7) (2005) 1155–1159.
- [28] T.T. Mills, G.E. Toombes, S. Tristram-Nagle, D.-M. Smilgies, G.W. Feigenson, J.F. Nagle, Order parameters and areas in fluid-phase oriented lipid membranes using wide angle X-ray scattering, *Biophysical J.* 95 (2) (2008) 669–681.
- [29] J. Seelig, W. Niederberger, Deuterium-labeled lipids as structural probes in liquid crystalline bilayers. Deuterium magnetic resonance study, *J. Am. Chem. Soc.* 96 (7) (1974) 2069–2072.
- [30] K.M. Lee, N.V. Tabiryan, T.J. Bunning, T.J. White, Photomechanical mechanism and structure-property considerations in the generation of photomechanical work in glassy, azobenzene liquid crystal polymer networks, *J. Mater. Chem.* 22 (2) (2012) 691–698.
- [31] X. Tong, L. Cui, Y. Zhao, Confinement effects on photoalignment, photochemical phase transition, and thermochromic behavior of liquid crystalline azobenzene-containing diblock copolymers, *Macromolecules* 37 (9) (2004) 3101–3112.
- [32] S. Xiao, X. Lu, Q. Lu, B. Su, Photosensitive liquid-crystalline supramolecules self-assembled from ionic liquid crystal and polyelectrolyte for laser-induced optical anisotropy, *Macromolecules* 41 (11) (2008) 3884–3892.
- [33] C.T. Imrie, F.E. Karasz, G.S. Attard, Side-chain liquid-crystalline copolymers containing spacers of differing lengths, *Macromolecules* 25 (4) (1992) 1278–1283.
- [34] C. Li, J.-H. Yun, H. Kim, M. Cho, Light propagation and photoactuation in densely cross-linked azobenzene-functionalized liquid-crystalline polymers: contribution of host and concerted isomerism, *Macromolecules* 49 (16) (2016) 6012–6020.
- [35] J.J. Wie, K.M. Lee, T.H. Ware, T.J. White, Twists and turns in glassy, liquid crystalline polymer networks, *Macromolecules* 48 (4) (2015) 1087–1092.
- [36] R.W. Lenz, Synthesis and properties of thermotropic liquid crystal polymers with main chain mesogenic units, *Polym. J.* 17 (1) (1985) 105–115.
- [37] C. Barrett, A. Natansohn, P. Rochon, Cis-trans thermal isomerization rates of bound and doped azobenzenes in a series of polymers, *Chem. Mater.* 7 (5) (1995) 899–903.
- [38] D.H. Wang, J.J. Wie, K.M. Lee, T.J. White, L.-S. Tan, Impact of backbone rigidity on the photomechanical response of glassy, azobenzene-functionalized polyimides, *Macromolecules* 47 (2) (2014) 659–667.
- [39] C.S. Paik, H. Morawetz, Photochemical and thermal isomerization of azaromatic residues in the side chains and the backbone of polymers in bulk, *Macromolecules* 5 (2) (1972) 171–177.
- [40] K. Anderle, R. Birenheide, M. Eich, J.H. Wendorff, Laser-induced reorientation of the optical axis in liquid-crystalline side chain polymers, *Die Makromol. Chem. Rapid Commun.* 10 (9) (1989) 477–483.
- [41] Y. Wu, Y. Demachi, O. Tsutsumi, A. Kanazawa, T. Shiono, T. Ikeda, Photoinduced alignment of polymer liquid crystals containing azobenzene moieties in the side chain. 2. Effect of spacer length of the azobenzene unit on alignment behavior, *Macromolecules* 31 (4) (1998) 1104–1108.
- [42] C.D. Eisenbach, Isomerization of aromatic azo chromophores in poly (ethyl acrylate) networks and photomechanical effect, *Polymer* 21 (10) (1980) 1175–1179.